

## Five-layer reverse tape casting of IT-SOFC

Snowdon, Abigail L.; Jiang, Zeyu; Steinberger-wilckens, Robert

DOI:

[10.1111/ijac.13911](https://doi.org/10.1111/ijac.13911)

License:

Creative Commons: Attribution (CC BY)

*Document Version*

Publisher's PDF, also known as Version of record

*Citation for published version (Harvard):*

Snowdon, AL, Jiang, Z & Steinberger-wilckens, R 2021, 'Five-layer reverse tape casting of IT-SOFC', *International Journal of Applied Ceramic Technology*, vol. 19, no. 1, pp. 289-298.  
<https://doi.org/10.1111/ijac.13911>

[Link to publication on Research at Birmingham portal](#)

### General rights

Unless a licence is specified above, all rights (including copyright and moral rights) in this document are retained by the authors and/or the copyright holders. The express permission of the copyright holder must be obtained for any use of this material other than for purposes permitted by law.

- Users may freely distribute the URL that is used to identify this publication.
- Users may download and/or print one copy of the publication from the University of Birmingham research portal for the purpose of private study or non-commercial research.
- User may use extracts from the document in line with the concept of 'fair dealing' under the Copyright, Designs and Patents Act 1988 (?)
- Users may not further distribute the material nor use it for the purposes of commercial gain.

Where a licence is displayed above, please note the terms and conditions of the licence govern your use of this document.

When citing, please reference the published version.

### Take down policy

While the University of Birmingham exercises care and attention in making items available there are rare occasions when an item has been uploaded in error or has been deemed to be commercially or otherwise sensitive.

If you believe that this is the case for this document, please contact [UBIRA@lists.bham.ac.uk](mailto:UBIRA@lists.bham.ac.uk) providing details and we will remove access to the work immediately and investigate.

## RESEARCH ARTICLE

# Five-layer reverse tape casting of IT-SOFC

 Abigail L. Snowdon  | Zeyu Jiang | Robert Steinberger-Wilckens

Centre for Hydrogen and Fuel Cell Research, School of Chemical Engineering, University of Birmingham, Edgbaston, UK

## Correspondence

A. L. Snowdon, Centre for Hydrogen and Fuel Cell Research, School of Chemical Engineering, University of Birmingham, Edgbaston B15 2TT, UK.  
Email: [AXSI420@bham.ac.uk](mailto:AXSI420@bham.ac.uk)

## Funding information

Engineering and Physical Sciences Research Council (EPSRC), Grant/Award Number: EP/L015749/1; University of Birmingham

## Abstract

Tape casting is a well-established method for manufacturing thin ceramic layers with controllable thickness and porosity. This study investigates the potential of 10Sc1CeSZ material for the electrolyte and anode layers for intermediate-temperature solid oxide fuel cells (IT-SOFC) in an anode-supported cell (ASC) geometry. In order to use  $\text{La}_{0.6}\text{Sr}_{0.4}\text{Co}_{0.2}\text{Fe}_{0.8}$  Oxide (LSCF) cathode material, a  $\text{Gd}_{0.2}\text{Ce}_{0.8}$  Oxide (GDC) barrier layer is needed; however, thermal expansion coefficient mismatch results in delamination of the GDC from the electrolyte during high temperature sintering when fabricated by conventional tape casting procedures. For the first time, ASCs have been manufactured by a five-layer tape casting technique; barrier layer, novel composite layer, electrolyte, anode functional layer, and anode substrate. Ni-ScCeSZ composite cells were tested between 650 and 800°C in  $\text{H}_2:\text{N}_2$  fuel (85%  $\text{H}_2$ ) on the anode and air on the cathode to yield a maximum power density of .46 W/cm<sup>2</sup>. These results demonstrate the feasibility of this new five-layer tape casting technique to produce IT-SOFC.

## KEYWORDS

gadolinia-doped ceria, impedance, Ni-ScCeSZ, solid oxide fuel cell, tape casting

## 1 | INTRODUCTION

Solid oxide fuel cells (SOFCs) are well-known electrochemical devices capable of producing power at low emission levels and high efficiencies. In order to become fully commercial, it is important to reduce the production costs and increase the lifetime. Research over the last decade has focused on reducing the degradation of the materials,<sup>1</sup> optimizing microstructure<sup>2,3</sup> to deal with fuel flexibility<sup>4,5</sup> and reducing the operating temperature from over 800°C to below 700°C in order to minimize thermally activated degradation effects and thermal stresses.<sup>6–8</sup> At high temperatures, the formation of insulating layers between the electrolyte and cathode, more specifically, the reaction of strontium from the LSCF cathode and zirconia

from the electrolyte inhibits the migration of oxygen ions across the membrane by forming insulating  $\text{SrZrO}_3$ . The addition of a GDC barrier layer stops Sr migration.<sup>9</sup> Researchers, though, have highlighted the difficulties in manufacturing this barrier layer by the tape casting technique,<sup>10</sup> due to the mismatch of thermal expansion coefficients (TECs), which leads to the green tape GDC layer delaminating from the electrolyte upon high temperature sintering. In 2017, Mehranjani et al. discussed the impossibility of creating a bi-layer electrolyte by depositing a YSZ layer onto GDC due to the shrinkage mismatch.<sup>11</sup> Furthermore, preliminary studies on the residual stresses of YSZ and GDC by Atkinson et al. identify how the significant TEC of GDC weakens the zirconia electrolyte upon cooling from the fabrication temperature.<sup>12</sup>

This is an open access article under the terms of the [Creative Commons Attribution](https://creativecommons.org/licenses/by/4.0/) License, which permits use, distribution and reproduction in any medium, provided the original work is properly cited.

© 2021 The Authors. *International Journal of Applied Ceramic Technology* published by Wiley Periodicals LLC on behalf of American Ceramics Society

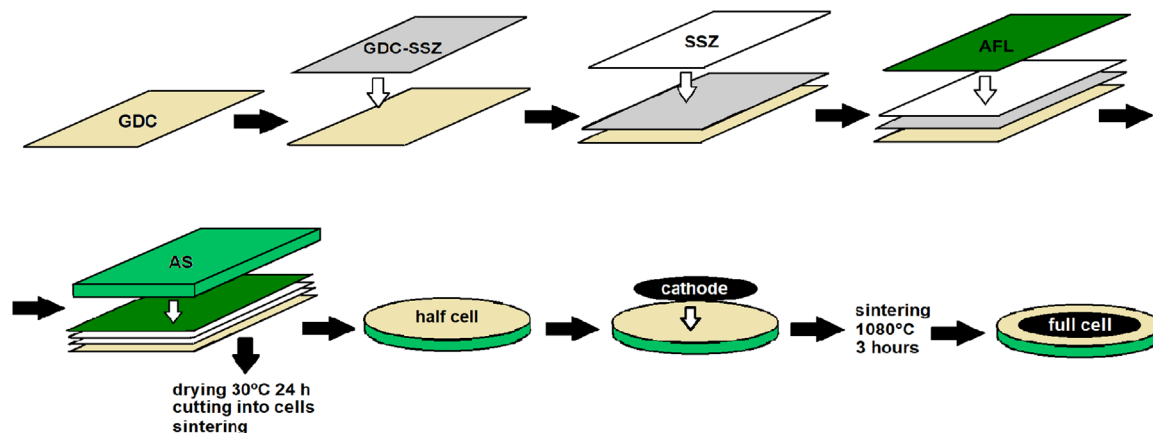


FIGURE 1 Order of casting layers in five-layer anode-supported SOC manufacturing. Scheme adopted from [Ref. 17](#)

Various methods of GDC deposition have been successfully used in the past, such as screen-printing and physical vapor deposition; however, they require additives that can reduce cell performance, have a higher cost, or are more time-consuming in comparison to tape casting.<sup>13</sup> In 2013, Song et al. found that the addition of a sintering aid to a screen printed GDC layer produced a dense barrier layer at higher sintering temperatures, but yielded a reduced electrochemical performance ( $.385 \text{ Wcm}^{-2}$ ) in comparison to a cell fabricated without any sintering aid ( $.86 \text{ Wcm}^{-2}$ ).<sup>14</sup> In 2018, a research group in France<sup>9</sup> demonstrated the ability of introducing a composite layer between a YSZ electrolyte and a GDC barrier layer through magnetron sputtering technique. They manufactured gradient deposits of GDC and YSZ to obtain cells that yielded  $.94 \text{ Wcm}^{-2}$ , compared to their screen printed cells,  $1.2 \text{ Wcm}^{-2}$ . However, the degradation rate for these magnetron sputtered cells was very high (18%/1000 h) due to poor adhesion of the sputtered layer.

Tape casting is a well-established, cost-effective method of producing homogeneous green tapes, and is the preferred method for mass production of SOCs due to the ability to produce layers with a range of thicknesses in a continuous process.<sup>15</sup> Therefore, in this work, tape casting has been chosen as the method of fabrication and a composite layer has been introduced in addition to the original electrolyte and barrier layers.

## 2 | EXPERIMENTAL PROCEDURE

### 2.1 | Preparation of NiO/ScCeSZ cells with composite layer electrolyte

The reverse tape casting approach established by Menzler et al.<sup>16</sup> was adapted to include a tape cast barrier layer and used in this work. The GDC layer was cast first, followed

by the composite layer, the electrolyte layer, and the anode functional layer (AFL), each layer being oven-dried in between casting at  $60^\circ\text{C}$  for 15 min. This was followed by casting the anode support (AS) and a final drying at  $30^\circ\text{C}$  for 24 h to produce a homogeneous green tape. The tape casting doctor blade gap height was chosen to obtain layers thick enough to prevent gas transfer between electrodes, but thin enough to minimize ohmic resistance within the cell. To densify the half cells, they were cosintered at  $1000^\circ\text{C}$  and then fully sintered at  $1400^\circ\text{C}$ . LSCF cathode ink was painted on the GDC side of the half cell and sintered at  $1080^\circ\text{C}$ . The completed cell was electrochemically tested to investigate the performance of the composite layer cell. Figure 1 illustrates the tape casting and cathode printing steps in sequence.

To produce a thin green tape, a Compact Tape Casting Film Coater with dryer and vacuum bed (MTI Corporation, Richmond, CA, USA) was used. The traverse speed and gap height of the doctor blade was variable to allow for different thickness of green tapes. The cells manufactured and tested in this work were based on NiO/YSZ and NiO/ScCeSZ material sets. The formulation was based upon previous work by Arifin et al.<sup>18</sup> A list of the materials used is presented in Table 1 describing their function, supplier, and measured particle size ( $d_{50}$ ).

For the anode substrate, the slurry consisted of 8YSZ or 10ScCeSZ precalcined at 800 and  $900^\circ\text{C}$  for 5 h, respectively, with as-received NiO powder in a weight ratio of 65:35 (NiO:8YSZ or 10ScCeSZ, respectively). Solvent (water), dispersant (Dispex, BASF), cermet powders, and pore former were mixed together using spherical and cylindrical  $\text{ZrO}_2$  beads, at 120 rpm for 24 h. The AFL consisted of a 65:35 mixture of as-received NiO and as-received YSZ or ScCeSZ powders, mixed together with the same solvent, and homogenized at 120 rpm for 24 h. Binders, plasticizers I and II, and antifoam were added to each slurry and mixed for a further 12 h at 70 rpm. To eliminate any air bubbles,

**TABLE 1** Materials used in the anode-supported composite cells

Material	Function	$d_{50}$ Particle size ( $\mu\text{m}$ )	Supplier
NiO	Anode support (AS)	$8.101 \pm .0156$	Hart Materials, UK
NiO	Anode functional layer (AFL)	$.997 \pm .0214$	Hart Materials, UK
8YSZ	Electrolyte	$1.264 \pm .0101$	Tosoh, Japan
10Sc1CeSZ	Electrolyte	$.892 \pm .0393$	DKKK, Japan
10GDC	Barrier layer	$.768 \pm .0185$	Fuel Cell Materials, UK
LSCF	Cathode	$.897 \pm .0193$	Praxair

**TABLE 2** Composition of the anode layers

Materials	Function	Composition (wt%)	
		AFL	AS
NiO	Electronic phase	35.8	35.8
ScCeSZ or YSZ	Ionic phase	19.3	19.3
Tapioca starch	Pore former	–	1.5
BASF Dispex Ultra 4404®	Dispersant	1.0	1.0
Water	Solvent	35.4	29.9
Antifoam 204	Antifoam	.2	.2
PVA	Binder	4.1	5.4
PEG 200	Plasticizer I	2.7	3.45
Glycerol	Plasticizer II	1.4	3.45

both slurries were filtered and degassed for 24 h, followed by a phase of 50 rpm slow-roll for 2 h to ensure a homogeneous mixture. Table 2 denotes all materials used in the anode layers and their composition.

The compositions for the electrolyte, barrier, and composite layers are presented in Table 3. First, the solvent, dispersant, binder, antifoam, and plasticizer were mixed together at 120 rpm for 24 h. More binder, defoamer, and the corresponding layer material powder were added and homogenized for at least 4 h at 120 rpm. To eliminate any air bubbles, the slurries were filtered and degassed for 1 h.

## 2.2 | Cathode ink preparation

To prepare the cathode ink, LSCF and GDC were combined in a 50:50 wt% ratio. Ink vehicle (Fuel Cell Materials) was added to the powder to make an ink with a solid loading of 59.70 wt%. LSCF ink was made by mixing LSCF powder with the ink vehicle to get a solid loading of 67.04 wt%. Both inks were homogenized using a triple roll mill (EXAKT).

## 2.3 | Characterization

The morphology of the cells was characterized by scanning electron microscopy (SEM) using a Hitachi table-top microscope TM3030Plus. Both cross-section and surface morphology micrographs were performed to examine the

microstructure. Image analysis was used to determine the thickness of each layer and the particle size. Energy dispersive X-ray (EDX) images were taken using back-scattered electrons to identify the elemental distribution throughout the cell. Particle size analysis after sintering was determined using ImageJ software. TECs were determined using a Dilatometer 402C (Netzsch) in the temperature range 298–1073 K in an air atmosphere. Sintered rods of each material were prepared by uniaxial pressing at 2 tones held for 2 min to yield samples of 7.8 mm diameter and 2.63 mm length, 7.59 mm diameter and 2.65 mm length, and 7.61 mm diameter and 2.71 mm in length for YSZ, ScCeSZ, and GDC, respectively. These samples were heated to 1400°C at 5 K min<sup>-1</sup>, held for 4 h, and then cooled to room temperature at 5 K min<sup>-1</sup>. A standard Al<sub>2</sub>O<sub>3</sub> rod of 6 mm diameter and 3 mm length was used as a reference sample. The coefficient of thermal expansion ( $\alpha$ ) is calculated from the initial length of the sample at room temperature,  $L$ , the change in length of the sample,  $dL$ , and the temperature,  $T$ , and is expressed in Equation (1):

$$\alpha = \left( \frac{dL}{dT} \right) / L. \quad (1)$$

AC impedance measurements were carried out with a Solartron 1470 E and 1455 FRA, sweeping from 10 kHz to .01 Hz, at an amplitude of 20 mA. Measurements were taken near OCV.

**TABLE 3** Composition of electrolyte, barrier, and composite layers

Materials	Function	Composition (wt%)		
		Barrier layer	Composite layer	Electrolyte
Water	Solvent	28	28	28
WB4101	Binder	19.3	19.3	19.3
DS001	Dispersant	2.0	2.0	2.0
DF002	Antifoam	.4	.4	.4
PL005	Plasticizer	.5	.5	.5
ScCeSZ or YSZ	Ionic phase	–	24.9	49.8
GDC	Barrier layer	49.8	24.9	–

**TABLE 4** Details of the differences in layers using the five-layer manufacturing technique

Name	GDC ( $\mu\text{m}$ )	Composite ( $\mu\text{m}$ )	Electrolyte ( $\mu\text{m}$ )	Total ( $\mu\text{m}$ )
Cell A	15.1	28.2	21.3	64.6
Cell 111	4.5	4.2	6.3	15.0
Cell 114	6.4	5.0	10.1	21.5
Cell 333	7.0	7.0	7.5	21.5

Table 4 illustrates the tape casting process of each layer and the relative layer thickness. The name denotes the gap height of the doctor blade used when tape casting, for example, Cell 111 used a gap height of 1  $\mu\text{m}$  for each layer, whereas Cell 114 used gap heights of 1, 1, and 4  $\mu\text{m}$  for GDC, composite, and electrolyte layers, respectively. All cells had an AFL and AS layer thickness of approximately 30 and 500  $\mu\text{m}$ , respectively.

To investigate their potential as SOCs, Ni-ScCeSZ composite electrolyte cells were electrochemically tested alongside likewise produced Ni-YSZ cells, further justifying the results against literature values and other cells made previously in the same research group.<sup>18</sup> The composite cells of both Ni-YSZ and Ni-ScCeSZ were fabricated into full anode-supported cells (ASCs) with a diameter 30 mm, and a cathode active area of 1.76 cm<sup>2</sup> fabricated with two layers; LSCF-GDC and LSCF. The cells were placed in the testing rig, and heated at 3°C/min to 800°C where they were reduced overnight. Both cells underwent initial characterization at 800°C, with 60 ml/min H<sub>2</sub> and 10 ml/min N<sub>2</sub> to the anode and 200 ml/min air to the cathode.

### 3 | RESULTS AND DISCUSSION

#### 3.1 | Thermal expansion coefficient

The TEC of the electrolyte and barrier layer materials was measured using the push-rod type dilatometer. In this

**TABLE 5** TEC values between 298 and 1073 K for YSZ, ScCeSZ, and GDC

Sample	TEC $\times 10^{-6}$ 1/K (298–1073 K)
8YSZ	10.72
10Sc1CeSZ	10.88
10GDC	13.84

work, we were interested in the TEC of the GDC barrier layer and the electrolyte layer (either YSZ or ScCeSZ) and their ability to sinter together without delamination, therefore, these three materials have been used in the measurement, and their TECs are presented in Table 5. The change in TEC between the electrolyte layer (YSZ or ScCeSZ) and the barrier layer (GDC) is  $3.12 \times 10^{-6}$  1/K between YSZ and GDC, and  $2.96 \times 10^{-6}$  1/K between ScCeSZ and GDC. These values can be used to explain the delamination seen upon high temperature sintering. TEC values are similar for YSZ and ScCeSZ due to the zirconia structure, explaining why this delamination is seen for both Ni-YSZ and Ni-ScCeSZ cells. A composite layer of 50:50 electrolyte materials and GDC was produced in an attempt to reduce this effect, minimizing the step change and therefore the delamination.

#### 3.2 | Composite layer

Figure 2 shows the SEM micrograph of a line scan taken of the cross-section of two cells: (A) before the addition of the composite layer, and (B) with the new composite layer. In Figure 2B the gradual transition from electrolyte to barrier layer can clearly be seen, and no delamination occurred after high temperature sintering.

Figure 3 presents the SEM micrographs of the different cells after sintering at 1400°C for 4 h. Figure 3A shows Cell A, the half-cell tape cast using a doctor blade gap height of 10  $\mu\text{m}$  each for the electrolyte, composite, and barrier layer. Cell A had an overall electrolyte-composite-barrier layer thickness of 64  $\mu\text{m}$ , 21.3  $\mu\text{m}$  being the electrolyte. This



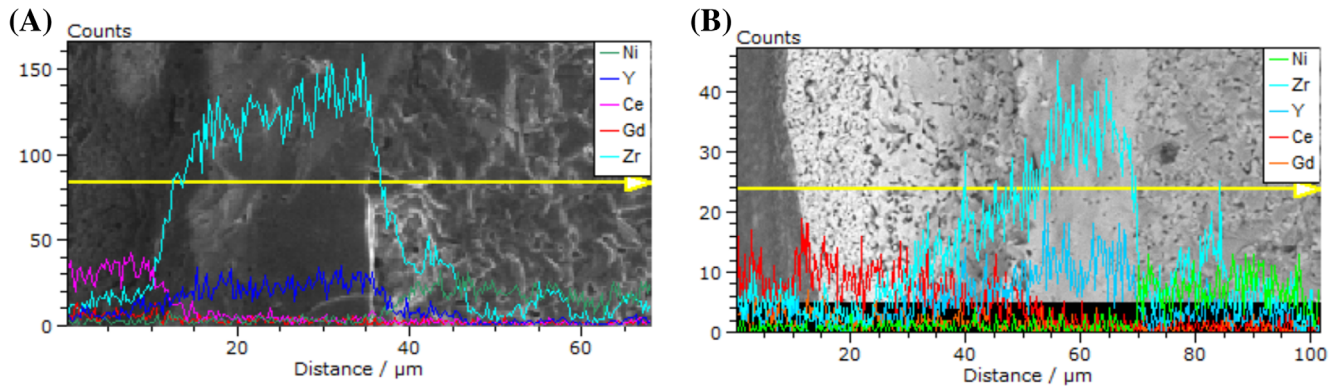


FIGURE 2 SEM line scans of the cross-section from (A) traditional Ni-YSZ cell and (B) a new five-layer cell

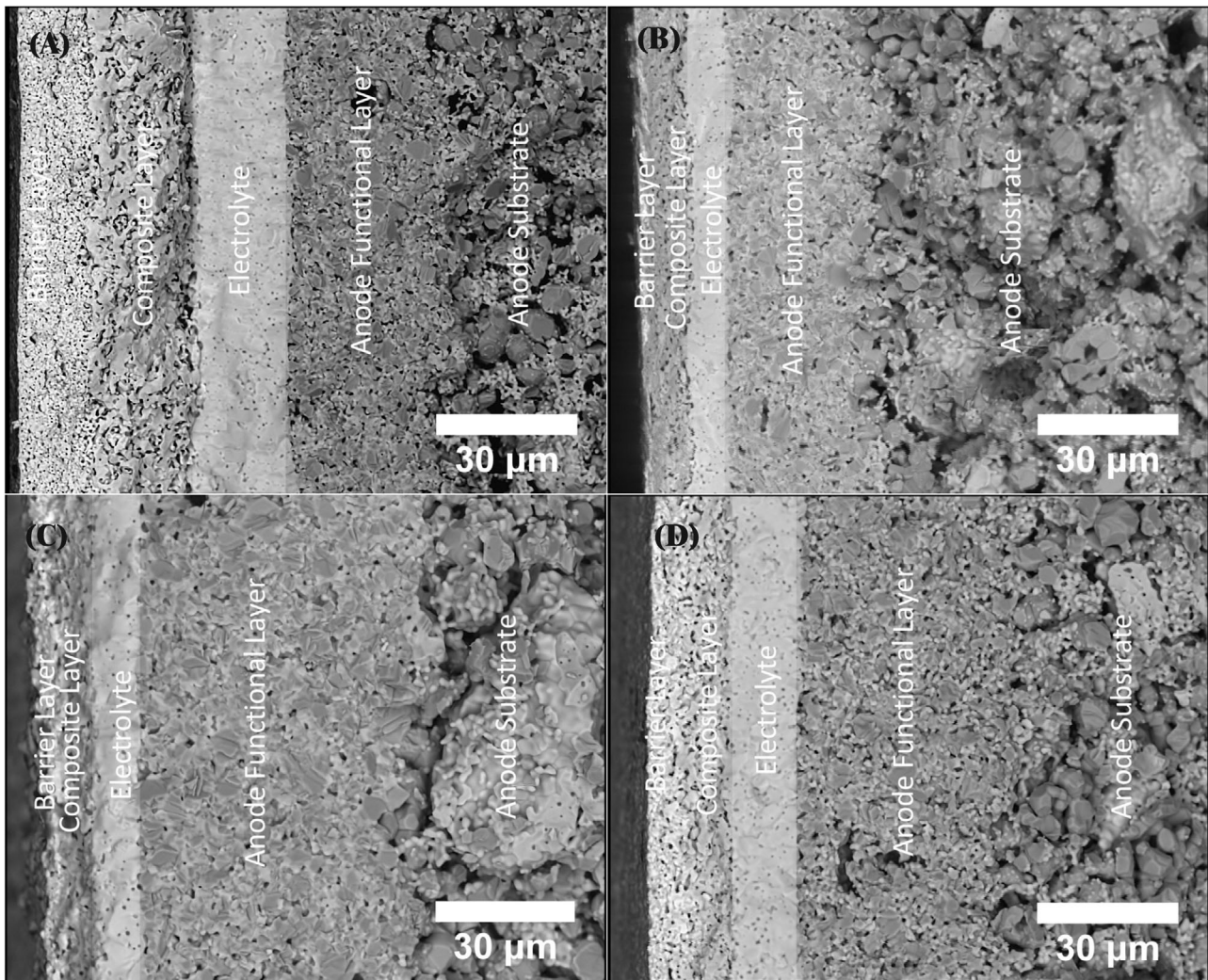


FIGURE 3 SEM micrographs of the composite layer for cross-section (A) Cell A: gap height of 10  $\mu\text{m}$ , (B) Cell 111, (C) Cell 114, and (D) Cell 333, after sintering for 4 h at 1400°C

was above the average thickness of ASC electrolytes of 10–15  $\mu\text{m}$ ,<sup>19</sup> resulting in a high ohmic resistance and poor performance. However, this cell was produced to confirm the approach of adding a composite layer and it is clear to see the dense electrolyte and the gradual transition to the barrier layer, with no cracks or delamination from the GDC barrier layer present after sintering.

In order to reduce the ohmic resistance, and further investigate the limits of the tape casting equipment, Figure 3B shows Cell 111, the half-cell, which was manufactured using the minimum doctor blade gap height of 1  $\mu\text{m}$  for each layer. After sintering, this resulted in an overall electrolyte-composite-barrier layer thickness of 15  $\mu\text{m}$ , 6.3  $\mu\text{m}$  of this being the electrolyte. Even though the tape casting equipment had been able to produce cells with acceptable layer thickness, Cell 111 resulted in poor performance and a reduced OCV value due to the thin electrolyte not densifying successfully during sintering, causing gas crossover and leakage during operation. Investigations into the optimal thickness of the three layers led to the fabrication of Cell 114 with a gap height for the GDC barrier layer and composite layer both set as 1  $\mu\text{m}$ , and the gap height for the electrolyte layer set as 4  $\mu\text{m}$ . The electrolyte thickness was increased to minimize gas leakage or crossover, and the composite layer kept to a minimum. After sintering, this resulted in an electrolyte thickness of 10  $\mu\text{m}$  and a combined thickness of 11  $\mu\text{m}$  for the composite and GDC layer. It is hypothesized that it is not the densification of the GDC barrier layer alone that is key in subduing the production of the  $\text{SrZrO}_3$  insulating layer, but the formation of a Zr-poor sublayer, which depends on sintering time and temperature,<sup>20</sup> hence, also keeping the GDC layer thickness to a minimum.

It was noted that when tape casting at the equipment's limit, 1  $\mu\text{m}$  gap width, holes in the tape appeared, most probably due to surface tension between the polyester film and the slurry, explaining the gas-crossover in Cell 111 and 114. After testing each gap height of the tape caster, it was concluded that these holes were less likely to appear when using a gap height of 2  $\mu\text{m}$ , and were completely absent when using a gap height of 3  $\mu\text{m}$ . Therefore, Cell 333 was manufactured using the minimum gap height without the appearance of holes in the layer.

During high-temperature sintering, it has been reported that the anode layers shrink more than the electrolyte layer, causing concave cell curvature.<sup>21</sup> To reduce this effect, presintering anode powders and a sintering temperature of 1280°C for the Ni-ScCeSZ cells had previously been used.<sup>18</sup> However, in this work, the addition of the GDC barrier layer required the sintering temperature to increase to 1400°C to ensure sufficient sintering of GDC. This increase in sintering temperature has the drawback of increasing interdiffusion between stabilized zirconia from the electrolyte and GDC barrier layer forming insulating

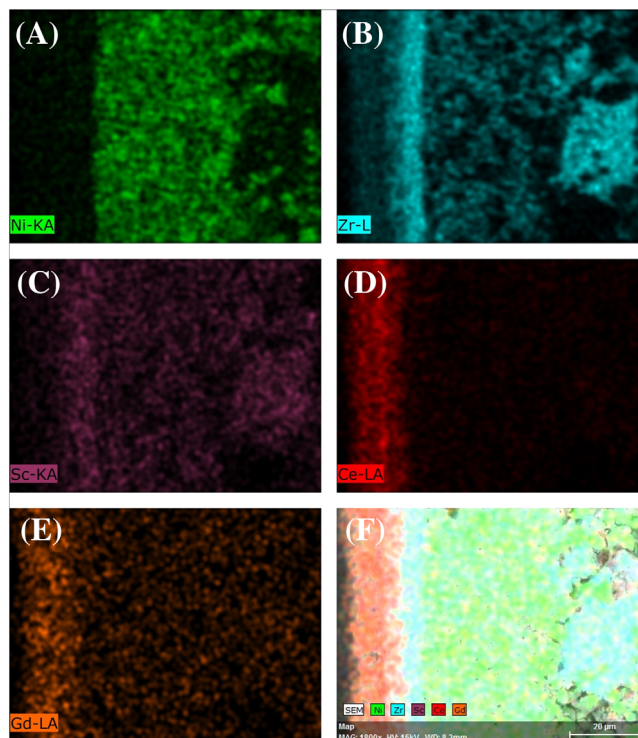


FIGURE 4 EDX elemental maps of the cross-section of a Ni-ScCeSZ composite half-cell, identifying (A) Ni, (B) Zr, (C) Sc, (D) Ce, (E) Gd, and (F) in the cross-section micrograph

layers, as described by Tsoga et al.<sup>22</sup> However, it has also been shown that sintering GDC at 1400°C with further sintering of the LSCF cathode at 1080°C leads to better performance than if the GDC was sintered at a lower temperature.<sup>20</sup>

After sintering at 1400°C for 4 h, the dense structure of the electrolyte and porous structure of the electrodes was observed as shown in Figure 3 and the GDC barrier layer was sintered without delamination. Figure 4 shows the elemental mapping and the distribution across each of the sintered layers. The GDC particle size was evaluated and the average particle size increased from 725 nm after sintering at 1350°C for 3 h to 1.062  $\mu\text{m}$  after sintering at 1450°C for 4 h. The increase in particle size with sintering temperature and time enabled the barrier layer to reduce pores that would otherwise facilitate the migration of Sr and, consequently, the formation of the  $\text{SrZrO}_3$  insulating layers.

Figure 5 illustrates the grain growth during sintering at different temperatures of the ScCeSZ electrolyte. Particle size analysis revealed an average particle size for tapes sintered at 1300, 1350, and 1400°C was 2.33, 4.09, and 8.16  $\mu\text{m}$ , respectively. The ionic conductivity of ScCeSZ increases with average grain size, hence, the half-cell sintering temperature of 1400°C for 4 h was chosen as it produced a dense electrolyte layer with the largest grain size.<sup>23</sup> These results are corroborated by other researchers.<sup>24</sup>



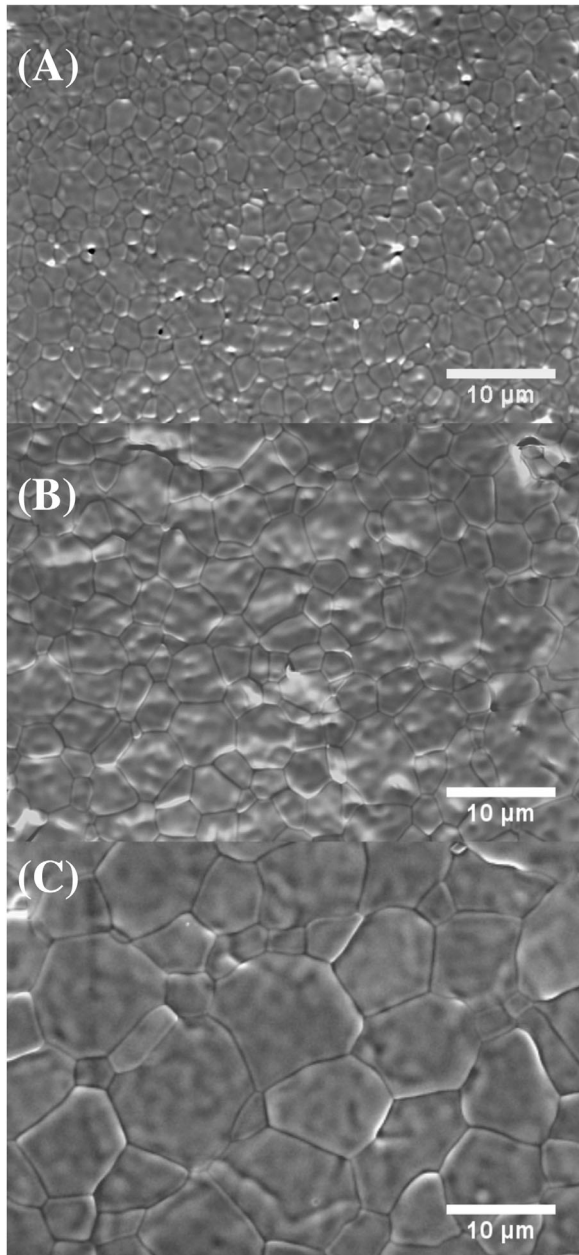


FIGURE 5 SEM micrographs of ScCeSZ pellets sintered at (A) 1300°C, (B) 1350°C, and (C) 1400°C for 4 h

### 3.3 | Electrochemical characterization

The initial cell performance was tested with 60 ml/min  $H_2$  and 10 ml/min  $N_2$  flow to the anode and 200 ml/min air flow to the cathode. The current–voltage curve was measured between 600 and 800°C in 50°C steps, from OCV and .4 V, and is shown in Figure 6. This yielded 400  $mWcm^{-2}$  at .7 V and a maximum power density 468  $mWcm^{-2}$  at 800°C. These performances can be compared to Ni-ScCeSZ cells manufactured in a similar way, with power densities of 390  $mWcm^{-2}$  at 750°C and Ni-YSZ cells with a power density of 530  $mWcm^{-2}$  at 800°C.<sup>18</sup>

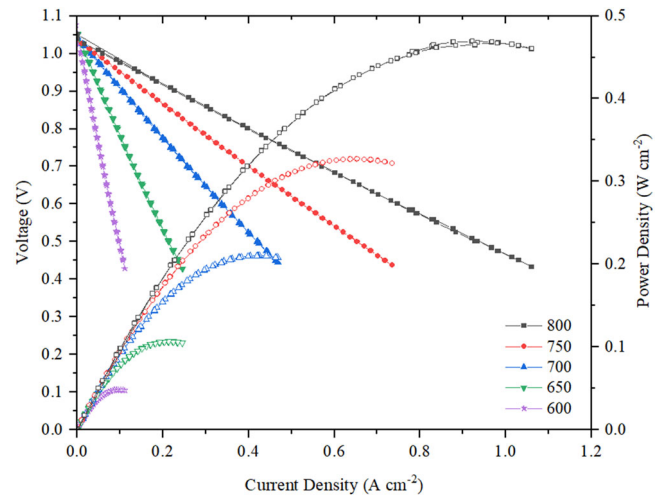


FIGURE 6 Performance of Cell 333: Ni-ScCeSZ composite cell prepared by five-layer tape casting tested between 600 and 800°C

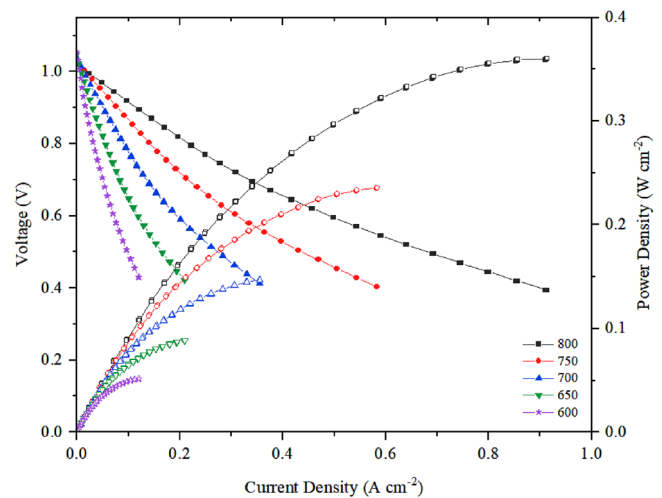


FIGURE 7 Performance of Cell 333: Ni-YSZ composite cell prepared by five-layer tape casting

Comparing Figures 6 and 7, the difference in performance of these two materials is proven at lower temperatures, as seen by the increased current density of the Ni-ScCeSZ cell and the lower internal resistances (Table 6). This behavior could point at a decisive influence of the cathode. It is well known that LSCF shows no advantage over other cathode materials at around 800°C, while performing considerably better at lower temperatures. Thus, the increased cathode polarization contribution at higher temperatures possibly masks the impact of the higher ionic conductivity of the electrolyte material.

Electrochemical impedance spectroscopy spectra reveal two overlapping semicircles at temperatures above 750°C and three at lower temperatures in the Nyquist plot in Figure 8. These are composed of the different processes; gas diffusion coupled with charge transfer and ionic transport



TABLE 6 Ohmic and polarization resistances taken from impedance measurements for both types of cell

Temperature (°C)	$R_s$ ( $\Omega \text{ cm}^2$ )		$R_{pol}$ ( $\Omega \text{ cm}^2$ )	
	Ni-ScCeSZ	Ni-YSZ	Ni-ScCeSZ	Ni-YSZ
800	.27	.09	.20	.76
750	.49	.14	.48	1.50
700	.63	.23	1.36	2.74
650	1.13	.42	3.75	5.07

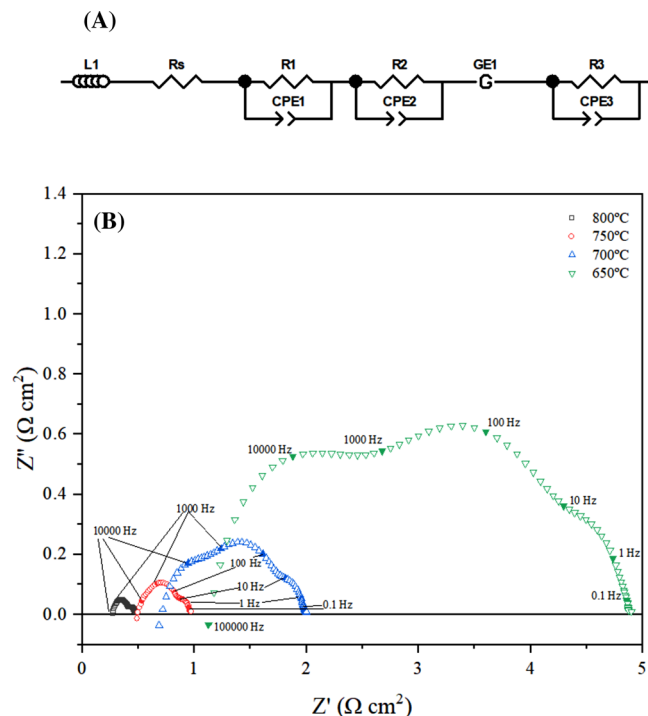


FIGURE 8 (A) Equivalent circuit model used in the CNLS fit of impedance data. (B) Electrochemical impedance data for NiScCeSZ cell taken at close to OCV at 800, 750, and 700°C using 60 ml/min  $\text{H}_2$  and 200 ml/min air

for the anode (1000–10 kHz) and cathode (100–1000 Hz), gas diffusion in the anode substrate (5–50 Hz) and oxygen diffusion in the cathode (5–0.1 Hz). The equivalent circuit used to analyze the Nyquist plot by complex nonlinear least squares (CNLS) fitting is shown in Figure 8A and consists of an inductor, resistor, two RQ elements (resistor and constant phase element in parallel) in series, a Gerischer element in series, and another RQ element. Similar models have been used by other researchers.<sup>25–28</sup> The ohmic resistance ( $R_s$ ) is taken as the high-frequency intercept of the x-axis and includes the ohmic contribution of the electrolyte and electrodes, the contact resistance between the electrodes and electrolyte, and the connections. The polarization resistance ( $R_{pol}$ ) is the difference between the  $R_s$  and the low-frequency intercept.

It is expected that the addition of a composite layer would increase the overall resistance at each tempera-

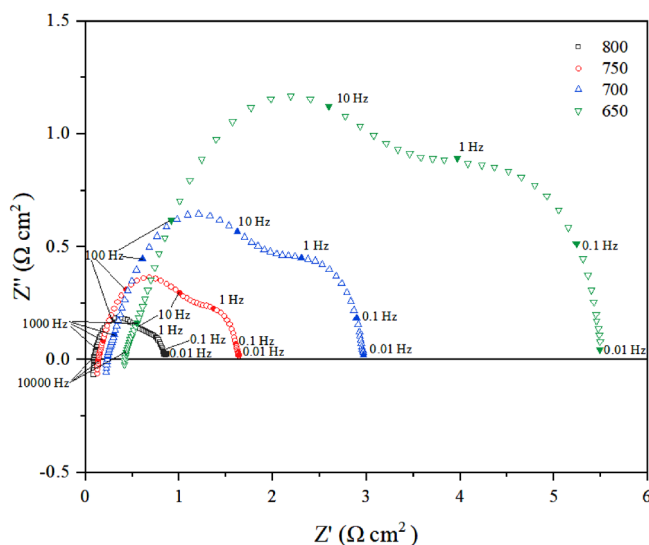


FIGURE 9 Impedance plot for NiYSZ cell taken close to OCV at 800, 750, 700, and 650°C using 60 ml/min  $\text{H}_2$ , 10 ml/min  $\text{N}_2$ , and 200 ml/min air

ture, hence, focus was laid on producing the thinnest possible composite layer via the tape casting equipment to minimize this resistance. As seen in Figure 9 the Ni-YSZ cell showed lower ohmic resistance compared to the Ni-ScCeSZ cell at all temperatures, but a higher polarization resistance. The larger  $R_s$  of the Ni-ScCeSZ could be an indication of inconsistent electrolyte layer thickness when manufacturing as the higher ionic conductivity of ScCeSZ would theoretically produce a lower  $R_s$ . The difference in  $R_s$  across the temperature range was much greater for the Ni-ScCeSZ cell, which displayed a range of  $\Delta R_s = .86 \Omega \text{ cm}^2$ , whereas the range for the Ni-YSZ cell was  $\Delta R_s = .33 \Omega \text{ cm}^2$ . Looking at the polarization resistance over the temperature range examined, the Ni-ScCeSZ cell outperformed the Ni-YSZ cell. The charge transfer resistance in the AFL was larger for the Ni-YSZ cell, which could point to microstructural irregularities within the anode, either incomplete reduction or inadequate porosity. At temperatures below 750°C, the Ni-ScCeSZ cell showed an increase in charge transport resistance, as seen by a third semicircle appearing at high frequency.

## 4 | CONCLUSION


The addition of an YSZ-GDC and ScCeSZ-GDC composite layer in the tape casting fabrication of Ni-YSZ and Ni-ScCeSZ SOCs has been proven. It has been possible to manufacture these layers, which successfully adhered to the electrolyte and GDC barrier layer for LSCF cathode cells, without delamination of the GDC barrier layer upon sintering.

After the functionality of the new composite layer was established with thin sheets of 20  $\mu\text{m}$ , the thickness of each layer was reduced down to 4  $\mu\text{m}$ , which established the limit of the tape casting instrument. This, however, resulted in poor OCV (.8 V) due to remaining porosity in the electrolyte layer and gas crossover during cell operation. The layer thicknesses were optimized to produce a cell with each layer thickness at 7  $\mu\text{m}$ . This composition resulted in a dense electrolyte with overall thickness of 21.5  $\mu\text{m}$ , including all three layers (electrolyte, composite, and barrier layer). These cells gave comparable OCV value to those from the literature (1.05 V) and a power density of 468  $\text{mWcm}^{-2}$  at 800°C. The polarization resistance at 800°C of the Ni-ScCeSZ and Ni-YSZ cell was .20 and .76  $\Omega \text{cm}^2$ , respectively, values which are larger than current state-of-the-art ASC from industry; however, this work proved the five-layer tape casting method eliminates the risk of delamination in producing working SOFCs. More research on optimizing these cells and their use with hydrocarbon fuels will be reported in the near future, including optimizing the composite layer to reduce the production of insulating layers between GDC and zirconia electrolytes during high-temperature sintering.

## ACKNOWLEDGMENTS

This work was performed within the Centre of Doctoral Training in Fuel Cells and Their Fuels, financially supported by the Engineering and Physical Sciences Research Council (EPSRC) under grant number EP/L015749/1 and by the University of Birmingham.

## ORCID

Abigail L. Snowdon  <https://orcid.org/0000-0001-5864-5459>

## REFERENCES

- Graves C, Ebbesen SD, Jensen SH, Simonsen SB, Mogensen MB. Eliminating degradation in solid oxide electrochemical cells by reversible operation. *Nat Mater*. 2014;14:239–44. <https://doi.org/10.1038/nmat4165>.
- Jiao Z, Takagi N, Shikazono N, Kasagi N. Study on local morphological changes of nickel in solid oxide fuel cell anode using porous Ni pellet electrode. *J Power Sources* 2011;196:1019–29. <https://doi.org/10.1016/j.jpowsour.2010.08.047>.
- Podhurs'ka VY. Structural changes in ScCeSZ-NiO ceramics in a high-temperature hydrogen environment. *Mater Sci*. 2010;46:129–31. <https://doi.org/10.1007/s11003-010-9307-z>.
- Blinn KS, Abernathy H, Li X, Liu M, Bottomley LA, Liu M. Raman spectroscopic monitoring of carbon deposition on hydrocarbon-fed solid oxide fuel cell anodes. *Energy Environ Sci*. 2012;5:7913–7. <https://doi.org/10.1039/C2EE21499G>.
- Mcintosh S, Gorte RJ. Direct hydrocarbon solid oxide fuel cells. *Chem Rev*. 2004;104:4845–6. <https://doi.org/10.1021/cr020725g>.
- Sadykov VA, Bobrenok OF, Irvine J, Vasylyev OD, Smirnova AL, Mezentseva NV, et al. Design of anode materials for IT SOFC: effect of complex oxide promoters and Pt group metals on activity and stability in methane steam reforming of Ni/YSZ (ScSZ) cermet. *J Fuel Cell Sci Technol*. 2010;7:6–11. <https://doi.org/10.1115/1.3117255>.
- Ishihara T, Shibayama T, Honda M, Nishiguchi H, Takita Y. Intermediate temperature solid oxide fuel cells using LaGaO3 electrolyte. *J Electrochem Soc*. 2000;147:1332–7. [https://doi.org/10.1115/S0013-4651\(99\)09-056-4](https://doi.org/10.1115/S0013-4651(99)09-056-4).
- Brett DJL, Atkinson A, Brandon NP, Skinner SJ. Intermediate temperature solid oxide fuel cells. *Chem Soc Rev*. 2008;37:1568–78. <https://doi.org/10.1039/b612060c>.
- Coddet P, Amany M-L, Vulliet J, Caillard A, Thomann A-L. YSZ/GDC bilayer and gradient barrier layers deposited by reactive magnetron sputtering for solid oxide cells. *Surf Coat Technol*. 2019;357:103–13. <https://doi.org/10.1016/J.SURFCOAT.2018.09.085>.
- McDonald NM. The manufacturing and testing of anode supported Ni10Sc1CeSZ SOFCs for intermediate temperature operation. 2017.
- Mehranjani AS, Cumming DJ, Sinclair DC, Rothman RH. Low-temperature co-sintering for fabrication of zirconia/ceria bi-layer electrolyte via tape casting using a Fe2O3 sintering aid. *J Eur Ceram Soc*. 2017;37:3981–93. <https://doi.org/10.1016/J.JEURCERAMSOC.2017.05.018>.
- Atkinson A, Selçuk A. Residual stress and fracture of laminated ceramic membranes. *Acta Mater*. 1999;47:867–74. [https://doi.org/10.1016/S1359-6454\(98\)00412-1](https://doi.org/10.1016/S1359-6454(98)00412-1).
- Menzler NH, Tietz F, Uhlenbruck S, Peter Buchkremer H, Stöver D. Materials and manufacturing technologies for solid oxide fuel cells. *J Mater Sci*. 2010;45:3109–35. <https://doi.org/10.1007/s10853-010-4279-9>.
- Song J-H, Jung MG, Park HW, Lim H-T. The effect of fabrication conditions for GDC buffer layer on electrochemical performance of solid oxide fuel cells. *Nano-Micro Lett*. 2013;5:151–8. <https://doi.org/10.5101/nml.v5i3.p151-158>.
- Mistler RE, Twiname ER. *Tape casting: theory and practice*. Ohio: Wiley; 2000.
- Menzler NH, Schafbauer W, Mücke R, Kauert R, Büchler O. Advanced manufacturing technology for solid oxide fuel cells. In: Bansal NP, Singh P, Widjaja S, Singh D, editors. *Advanced solid oxide fuel cells VII*. John Wiley & Sons, Ltd; 2011, p. 147–60. <https://doi.org/10.1002/9781118095249.ch14>.
- Blum L, De Haart LGJ, Malzbender J, Menzler NH, Rimmel J, Steinberger-Wilckens R. Recent results in Jülich solid oxide fuel cell technology development. *J Power Sources*. 2013;241:477–85. <https://doi.org/10.1016/j.jpowsour.2013.04.110>.

18. Arifin N, Button T, Steinberger-Wilckens R. Carbon-tolerant Ni/ScCeSZ via aqueous tape casting for IT-SOFCs. *ECS Trans.* 2017;78:1417–26. <https://doi.org/10.1149/07801.1417ecst>.
19. Basu RN, Das Sharma A, Dutta A, Mukhopadhyay J. Processing of high-performance anode-supported planar solid oxide fuel cell. *Int J Hydrogen Energy.* 2008;33:5748–54. <https://doi.org/10.1016/j.ijhydene.2008.06.073>.
20. Wilde V, Störmer H, Szász J, Wankmüller F, Ivers-Tiffée E, Gerthsen D. Gd 0.2 Ce 0.8 O 2 Diffusion Barrier Layer between (La 0.58 Sr 0.4 )(Co 0.2 Fe 0.8 )O 3– $\delta$  Cathode and Y 0.16 Zr 0.84 O 2 Electrolyte for Solid Oxide Fuel Cells: Effect of Barrier Layer Sintering Temperature on Microstructure. *ACS Appl Energy Mater.* 2018;1:6790–800. <https://doi.org/10.1021/acsaem.8b00847>.
21. Arifin NA. *Developing carbon tolerant Ni/ScCeSZ cells via aqueous tape casting for direct biogas fed solid oxide fuel cells (SOFC).* University of Birmingham; 2018. <https://doi.org/10.1017/CBO9781107415324.004>.
22. Tsoga A, Gupta A, Naoumidis A, Nikolopoulos P. Gadolinia-doped ceria and yttria stabilized zirconia interfaces: regarding their application for SOFC technology. *Acta Mater.* 2000; 48:4709–14. [https://doi.org/10.1016/S1359-6454\(00\)00261-5](https://doi.org/10.1016/S1359-6454(00)00261-5).
23. Escardino A, Belda A, Orts MJ, Gozalbo A. Ceria-doped scandia-stabilized zirconia (10Sc2O3-1CeO2-89ZrO2) as electrolyte for SOFCs: sintering and ionic conductivity of thin, flat sheets. *Int J Appl Ceram Technol.* 2017;14:532–42. <https://doi.org/10.1111/ijac.12675>.
24. Ramesh S, Ng CK, Tan CY, Wong WH, Ching CY, Muchtar A, et al. Effects of sintering on the mechanical and ionic properties of ceria-doped scandia stabilized zirconia ceramic. *Ceram Int.* 2016;42:14469–74. <https://doi.org/10.1016/j.ceramint.2016.06.050>.
25. Yoo Y-S, Choi M, Hwang J-H, Im H-N, Singh B, Song S-J. La2NiO4 as oxygen electrode in reversible solid oxide cells. *Ceram Int.* 2015;41:6448–54. <https://doi.org/10.1016/j.ceramint.2015.01.083>.
26. Shin E-C, Ahn P-A, Seo H-H, Nguyen DT, Kim S-D, Woo S-K, et al. Pinning-down polarization losses and electrode kinetics in cermet-supported LSM solid oxide cells in reversible operation. *Solid State Ionics.* 2015;277:1–10. <https://doi.org/10.1016/J.SSI.2015.04.009>.
27. Leonide A. *SOFC modelling and parameter identification by means of impedance spectroscopy.* Karlsruhe: Karlsruhe Institut für Technologie Scientific Publishing; 2010.
28. Papurello D, Menichini D, Lanzini A. Distributed relaxation times technique for the determination of fuel cell losses with an equivalent circuit model to identify physicochemical processes. *Electrochim Acta.* 2017;258:98–109. <https://doi.org/10.1016/j.electacta.2017.10.052>.

**How to cite this article:** Snowdon AL, Jiang Z, Steinberger-Wilckens R. Five-layer reverse tape casting of IT-SOFC. *Int J Appl Ceram Technol.* 2021;1-10. <https://doi.org/10.1111/ijac.13911>